Journal of Alloys and Compounds 650 (2015) 848–852

Contents lists available at ScienceDirect

Journal of Alloys and Compounds

journal homepage: http://www.elsevier.com/locate/jalcom

Soft X-ray absorption spectroscopy study of $(Ba_{0.5}Sr_{0.5})(Co_{0.8}Fe_{0.2})_{1-x}Nb_xO_{3-\delta}$ with different content of Nb (5%–20%)

Y.V. Egorova [a, *], T. Scherb [b], G. Schumacher [b], H.J.M. Bouwmeester [c], E.O. Filatova [a]

[a] Institute of Physics, St-Petersburg State University, Ulyanovskaya Str. 3, Peterhof 198504, St. Petersburg, Russia
[b] Helmholtz-Zentrum Berlin für Materialien und Energie GmbH, Hahn-Meitner-Platz 1, D-14109 Berlin, Germany
[c] University of Twente, P.O. Box 217, 7500 AE Enschede, The Netherlands

ARTICLE INFO

Article history:
Received 31 May 2015
Received in revised form
9 August 2015
Accepted 10 August 2015
Available online 13 August 2015

Keywords:
Solid oxide fuel cell
Microstructure
Local bonding environment
Near edge X-ray absorption fine structure

ABSTRACT

The mixed electronic ionic conducting materials $(Ba_{0.5}Sr_{0.5})(Co_{0.8}Fe_{0.2})_{1-x}Nb_xO_{3-\delta}$ with partial Nb substitution (x: 0.05, 0.10, 0.15, 0.20) for B cations (Co/Fe), synthesized using a solid state reaction method, have been studied by near edge X-ray absorption fine structure (NEXAFS). Co $L_{2,3}$- absorption spectra of $(Ba_{0.5}Sr_{0.5})(Co_{0.8}Fe_{0.2})_{1-x}Nb_xO_{3-\delta}$ (BSCFN) powders were analyzed with the purpose to understand the influence of the Nb substitution on the atomic electronic structure of BSCFN. The joint analysis of the Co $L_{2,3}$- absorption spectra reveals the presence of mixed oxidation states Co^{2+}/Co^{3+} in all the studied BSCFN structures. It was established that the proportion of oxidation states Co^{2+}/Co^{3+} and the corresponding coordinations of Co atoms depend on the content of Nb. In the 10% Nb substituted BSCF sample Co atoms mostly occur in the Co^{2+} oxidation state and are preferentially characterized by an octahedral coordination site. In all other structures Co atoms are rather characterized by Co^{2+}/Co^{3+} oxidation states and occupy both octahedrally and tetrahedrally coordinated sites.

1. Introduction

Due to their good oxygen exchange performance, the highest oxygen permeation and mixed ionic and electronic conductivity, $Ba_{0.5}Sr_{0.5}Co_{0.8}Fe_{0.2}O_{3-\delta}$ (BSCF) oxides are potential candidates for cathode materials in solid oxide fuel cell (SOFC) application [1,2]. BSCF is an oxide mineral with a perovskite structure (schematic formula of ABO_3). Ideal perovskites are characterized by a cubic crystal structure. Cations in the B position have an octahedral coordinations of oxygen anions and the voids between neighboring octahedra are filled with A-cations, coordinated by 12 oxygen ions. The crystal structure of perovskites depends on the ionic radii of oxygen anions and the cations. Goldschmidt introduced a tolerance factor (t), showing the deviation from the ideal cubic perovskite structure [3]:

$$t = \frac{r_A + r_O}{\sqrt{2}(r_B + r_O)},$$

where r_A, r_B, and r_o are the ionic radii of the A- and B- cations and of the oxygen anions, respectively. The cubic perovskite structure is preferred when $0.8 < t < 1$, while the formation of the hexagonal structure is preferred for $t > 1$. Analysis of BSCF structures shows that depending on the oxidation of the B-site cation, the tolerance factor of $Ba_{0.5}Sr_{0.5}Co_{0.8}Fe_{0.2}O_{3-\delta}$ varies within $0.97 < t < 1.07$ [4–6]. The mixed ionic and electronic BSCF conductors generally keep a significant concentration of oxygen vacancies (δ) [4,7,8]. A significant number of mobile oxygen vacancies makes BSCF an excellent oxygen conductor and a good candidate for solid oxide fuel cell (SOFC) applications [8,9] in the high temperature regime.

However, at intermediate temperatures (500°C–800°C) BSCF suffers from a slow decomposition of the cubic phase into a Co- and Ba enriched hexagonal phase and a cubic phase depleted in Co and Ba, resulting in a strong reduction of its performance [9,10]. As follows from Refs. [9–11], the instability of cubic BSCF at intermediate temperatures is predominantly connected with oxidation instability of the transition metal cations (mainly Co).

One way to solve the problem of phase stability of BSCF at

* Corresponding author.
E-mail addresses: Startjuli@gmail.com (Y.V. Egorova), tobias.scherb@helmholtz-berlin.de (T. Scherb), schumacher@helmholtz-berlin.de (G. Schumacher), h.j.m.bouwmeester@tnw.utwente.nl (H.J.M. Bouwmeester), elenaofilatova@mail.ru (E.O. Filatova).

http://dx.doi.org/10.1016/j.jallcom.2015.08.073
0925-8388/

intermediate temperatures is partial substitution of Nb for Co and Fe [5,11–13]. The stabilization effect of Nb for BSCF perovskite structures stems from the difference between interatomic distances in cubic and hexagonal perovskite structures. The distances between the Co/Fe ions and the oxygen ions (Co–O and Fe–O) in the hexagonal structure are shorter than in the cubic phase [13,14]. In accordance with the law of charge neutrality maintenance, the substitution of Nb^{5+} for Co atoms in BSCF system will lead to a valence reduction of B-site elements and/or a decrease in the concentration of oxygen vacancies. The lowering of the B-site element oxidation state leads to an increase of its ionic radius and thus to an increase in the bond length [13]. As a consequence of the substitution of Nb for (Co/Fe), B-site cations will preferentially take the cubic structure with longer distances between B cations.

It can be assumed that the substitution of Nb^{5+} for Co/Fe atoms in a BSCF system, leading to valence reduction of B-site elements and/or a decrease in the concentration of oxygen vacancies, can be accompanied not only by a change in the interatomic distance Co–O and Fe–O but also by the alteration of the coordination number and local environment of the B- cation.

It has been recently shown [11], that substitution of Nb for the B-site cations effectively improved the chemical stability of BSCF under high oxidation condition.

Traditionally, BSCF compounds are investigated using the extended X-ray absorption fine structure (EXAFS) method. It is well known that EXAFS is due mostly to single scattering events of high-energy photoelectrons off the atomic cores by the neighboring atoms [15]. At the same time, when talking about identifying the distortion of the nearest environment of the central atom, the NEXAFS studies seem appropriate. The NEXAFS arises from excitations from core levels into unoccupied molecular orbitals and is dominated by multiple scattering of a low-energy photoelectron in the valence potential set up by the nearest neighbors. Often one can use a spectral "fingerprint" technique to identify the local bonding environment that defines the highest sensitivity of NEXAFS to distinguish chemical bonds and nearest polyhedral coordination sites. Thus NEXAFS provides the information about local (associated with a hole localization in the core shell) and partial (allowed for certain angular momentum symmetry) electronic density of states of the conduction band.

In this connection we have attempted to study the $(Ba_{0.5}Sr_{0.5})(Co_{0.8}Fe_{0.2})_{1-x}Nb_xO_{3-\delta}$ perovskites with partial Nb substitution for Co/Fe depending on the amount of Nb using NEXAFS. The goal of the current work is a study of the effect of Nb substitution of the B-site elements on the lowest unoccupied electronic states of the BSCF systems and as a consequence on the B coordination sites in the $(Ba_{0.5}Sr_{0.5})(Co_{0.8}Fe_{0.2})_{1-x}Nb_xO_{3-\delta}$ structure.

2. Experimental

All specimens of the mixed electronic ionic conducting materials $(Ba_{0.5}Sr_{0.5})(Co_{0.8}Fe_{0.2})_{1-x}Nb_xO_{3-\delta}$ with partial Nb substitution (x: 0.05, 0.10, 0.15, 0.20) for B-cations (Co/Fe) were synthesized nominally in the same way using a solid state reaction method. After synthesizing the powder mixtures were dried, calcined in air at 950 °C and 1000 °C for 10 h at each temperature with intermediate milling in a mortar for 2 h [12]. In the following, these materials will be denoted as BSCFN05, BSCFN10, BSCFN15, and BSCFN20, respectively. The NEXAFS measurements were performed at the RGL-station (the Russian–German beamline) at the BESSY II synchrotron light source of the Helmholtz-Zentrum Berlin [16]. The spectra were measured at the incident angle of 45° in the vicinity of Co $L_{2,3}$- and Fe $L_{2,3}$- absorption edges with energy resolution better than $E/\Delta E = 2000$. The spectra were obtained by monitoring the total electron yield (TEY) from the samples in the current mode. The energy scale was referenced to Au 4f 7/2 photoelectron peak (83.95 eV).

Angle dispersive X-ray diffraction (XRD) measurements were carried out with a *Bruker D8 Advance* diffractometer using Cu Kα radiation (wavelength $\lambda = 0.154$ nm).

3. Results and discussion

The Co $L_{2,3}$- and Ba $M_{4,5}$- absorption spectra of Nb-substituted BSCF samples are shown in Fig. 1. The relative intensities of all the Co $L_{2,3}$- and Ba $M_{4,5}$- absorption spectra have been normalized to the continuum jump at the photon energy of 810 eV, after subtraction of a sloping background, which was extrapolated from the linear region below the Co $L_{2,3}$- and Ba $M_{4,5}$- absorption onset. All the studied absorption spectra consist of two groups of features A–B and A*–B*. The energy distances A–A* = 14.4 eV and B–B* = 14.7 eV agree well with the spin–orbit splitting of the Co 2p- and Ba 3d - levels in BSCF [17], respectively. The Co $2p_{1/2}$- and Ba $3d_{3/2}$- structures are marked by asterisks in Fig. 1. A joint analysis of all the studied spectra of BSCF samples does not reveal any visible differences in the shape and/or energy position of the features corresponding to Ba $M_{4,5}$- absorption spectrum (B and B*). On the other hand the shape of the spectra in the vicinity of the Co $L_{2,3}$- absorption edge depends on the Nb-content. The effect is more pronounced in the Co L_3-than in the L_2-absorption spectra. It is well known that the L_2 absorption spectra is misrepresented by an additional damping channel caused by the L_2L_3V- Coster–Kronig transition [18], which leads to the shorter life time of L_2-holes. We will, therefore, focus on the analysis of the evolution of the Co $2p_{3/2}$ -absorption spectra.

The evolution of the shape of the Co $2p_{3/2}$- (Co L_3-) absorption spectra of Nb-substituted BSCF samples are shown in Fig. 2. Bearing in mind that the absorption spectra fine structure is very sensitive to the nature of the absorbing atoms, the chemical state and local coordination environment, it may be expected to be a manifestation of different oxidation states of the Co atoms in the Co L_3-absorption spectrum. The energy position of the metal L-edge shifts towards higher energies with an increase of its oxidation state [9,19].

To understand the observed changes in the Co L_3-absorption spectrum, the Co-L_3 absorption spectra of CoO- (oxidation state Co^{2+}) and Co_3O_4- (oxidation states Co^{3+}/Co^{2+}) structures were also analyzed (Fig. 2). The Co L_3-absorption spectrum of CoO was

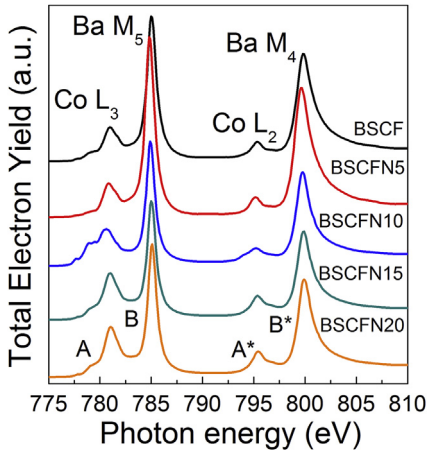

Fig. 1. Co $L_{2,3}$- and Ba $M_{4,5}$- absorption spectra of BSCF systems with partial (5%, 10%, 15% and 20%) Nb substitution for B-site atoms. The details A and A* denote to Co $2p_{3/2}$ and Co $2p_{1/2}$, details B and B* denote to Ba $3d_{5/2}$- and Ba $3d_{3/2}$- levels, respectively.

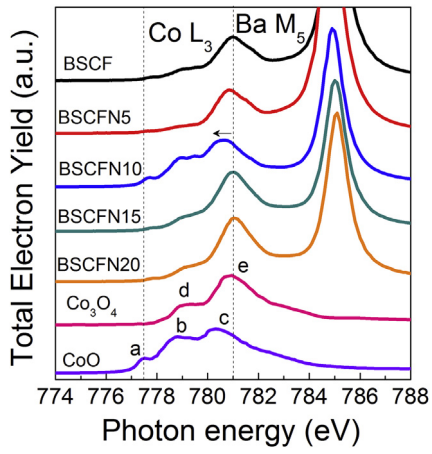

Fig. 2. Co L_3-absorption spectra of Nb substituted BSCF systems, compared with Co L_3-absorption spectra of CoO and Co_3O_4 systems. The absorption spectrum of Co_3O_4 is taken from Ref. [9]. The denotations **a**–**d** used to describe features of Co L_3-absorption spectra are explained in the text.

measured under the same experimental conditions as the absorption spectra of the Nb substituted BSCF samples whereas the Co L_3-absorption spectrum of Co_3O_4 was taken from Ref. [9].

In terms of the crystal field theory the energy levels of d-orbitals of the cation are split under the octahedrally (tetrahedrally) coordinated ligand-field into $t_{2g}(e_g)$ and $e_g(t_{2g})$ orbitals. As a result, both L_3 (and L_2) features are further split into doublet features. When comparing CoO and Co_3O_4 compounds, the balance between the crystal field splitting (Δ) (i.e., the energetic splitting between t_{2g}- and e_g- orbitals) and the exchange interaction (J) associated with Hund's rule should be considered [20,21]. Depending on the values of Δ and J the electrons are redistributed differently between the t_{2g}- and e_g- orbitals producing the different spin configurations.

CoO has a cubic crystal structure in which the Co^{2+}- ions are located in octahedral coordination (O_h) [20,22,23]. The ground state of Co^{2+} has an [Ar] $3d^74s^0$ configuration. According to the classical conception, the Co $2p_{3/2}$- absorption spectrum of CoO shows dipole allowed transitions of Co $2p_{3/2}$- electrons to unoccupied 3d states split by the octahedral crystal field created mainly by the O atoms [23,24]. The crystal field in CoO is relatively weak (the crystal field value (10Dq) of the ground state is ~1 eV [21]) that causes a high-spin configuration $t^5_{2g}e^2_g$ where the t_{2g}- orbitals are partly filled and therefore allow for low-energy d–d excitations. The ground term of the ground state of the Co^{2+} ion is ^4F, which is split on $^4T_{1g}$ (F), $^4T_{2g}$, $^4A_{2g}$ [21] features, and this explains the presence of the features **a**–**c** in the Co $L_{2,3}$- absorption spectrum of CoO (Fig. 2). Note that in a pure octahedral symmetry the crystal field value 10Dq is given by the energy difference between the $^4T_{2g}$ (4F) and the $^4A_{2g}$ (4F) states, and not by the energy difference between $^4T_{1g}$ (4F) and $^4T_{2g}$ (4F), as $^4T_{1g}$ (4F) is hybridized with the $^4T_{1g}$ (4P) states [25,26].

In Co_3O_4 which has spinel-type structure cobalt ions exist in two different oxidation states, Co^{2+} and Co^{3+}. Co atoms can, therefore, occupy both octahedrally coordinated sites (16 sites for Co^{3+}) and tetrahedrally coordinated sites (8 sites for Co^{2+}) with the ratio 2:1 [27]. In Co_3O_4, the tetrahedral sites are occupied by Co^{2+} with a high-spin state configuration $e^4_gt^3_{2g}$ (the ground term is $^4A_{2g}$) while the octahedral sites are occupied by Co^{3+} with a low-spin state configuration $t^6_{2g}e^0_g$ (S = 0, the ground term is $^1A_{1g}$). We stressed that in tetrahedral coordination there is the energetically reversed order of e_g and t_{2g} components compared with octahedral coordination. One can conclude that the Co $L_{2,3}$- absorption spectrum of Co_3O_4 corresponds to a mixture of Co^{3+} and Co^{2+} oxidation states (with ratio of 2:1). According to [23], the feature **d** of the Co $L_{2,3}$- absorption spectrum of Co_3O_4 reflects predominantly the Co^{2+}- states and feature **e** is formed mainly from the Co^{3+}- states.

The joint analysis of the absorption spectra of all the studied BSCF structures in Fig. 2 reveals that the shape of the Co L_3-absorption spectrum depends on the Nb-substitution in the B position. The most noticeable changes are traced in the Co L_3-absorption spectrum of BSCFN10: i) the spectrum is shifted towards lower energies by about 0.5 eV with respect to the spectra of all the other samples; ii) more higher intensity of a shoulder denoted by (**a**) in Fig. 2, which is hardly visible in the spectra of the other specimens. In the number of features and their energy positions the Co $L_{2,3}$- absorption spectrum of BSCF samples with 10% Nb substitution Co atoms correlates well with the Co L_3-absorption spectrum of CoO where the Co^{2+} ions are located in octahedral coordination. The spectra of all the other BSCF samples are more similar to the Co L_3-absorption spectrum of Co_3O_4 with a small part of the Co L_3-absorption spectrum of CoO (appearance of the weak feature **a**).

It is plausible to assume that the Co oxidation state in Nb substituted BSCF depends on the Nb content. The change of the Co oxidation state is greater in BSCFN10 than in all the other samples. The joint analysis of the Co L_3-absorption spectra of all the studied BSCF structures reveals that in the BSCF samples with 5, 15, 20% Nb substitution, Co atoms occupy sites with mixed oxidation states Co^{2+}/Co^{3+} and as a consequence, octahedrally and tetrahedrally coordinated sites. Co atoms in BSCFN10 are predominantly characterized by a valence of 2^+ and occupy predominantly octahedrally coordinated sites.

The possibility of phase transformation from Co_3O_4 to CoO was traced in different NEXAFS [28] and XPS [29] studies. In particular, according to [29], the main peaks of Co $2p_3/_2$ and Co $2p_1/_2$ in CoO upshift by 0.8 eV in contrast to Co_3O_4. This shift is due to the change of the coordination environment of Co ions from Co_3O_4 to CoO. This observation is an additional evidence of our conjecture that Co atoms in BSCF sample with 10% Nb substitution are predominantly characterized by a valence of 2^+.

In an orderly sequence of BSCF with partial Nb substitution of model BSCF, BSCFN05, BSCFN10, BSCFN15 and BSCFN20 the branching ratio I_2/I_3 (where I_2 and I_3 are the integral intensities of the L_2 and L_3 peaks, respectively) for Co $L_{2,3}$-absorption edges is equal to 0.40, 0.41, 0.27, 0.43 and 0.43, respectively. The uncertainty is about 0.05, and is specified by the accuracy determining the values of the intensities and also by the accuracy of elicitation of the Ba-$M_{4,5}$- absorption spectra features and, as a consequence, by accuracy of background subtraction for Co $L_{2,3}$-absorption spectra features. It is evident that in the considered sequence the ratio L_2/L_3 is near 0.4 and decreases to value of ~0.3 for BSCF with 10% Nb substitution.

Within the independent particle approximation the so-called branching ratio between the L_2 and L_3 edges is determined by the occupation numbers of the corresponding core states and gives 1:2 [30]. However, according to [30,31], a deviation of the branching ratio L_2/L_3 from its statistical value in 3d elements is traced. A similar problem of the ratio between the L_β- and L_α-line intensities of 3d transition metal oxides was studied in X-ray emission spectra [18]. In Ref. [18] the existence of the integrated-intensity ratio of L_β- and L_α-lines on the atomic magnetic moment has been established.

The deviation of the branching ratio L_2/L_3 from its statistical value is due to the interaction of the exited electron with its core hole (due to the localization of the core wave function), which is very strong in the case of 3d-elements and cannot be ignored. It is important that according to [31], the exchange term does not depend on the screening but is related to a coherent mixing between the excitations from $2p_{1/2}$- and $2p_{3/2}$- core levels in 3d-elements. As follows from the [31] this effect is proportional to the size

of the spin–orbit splitting and becomes smaller for later transition metals. For titanium oxides, as an example, the ratio L_2/L_3 is close to 1:1. With respect to late transition metal compounds, according to [32] the number of unpaired 3d-electrons reduces in the creation of the core hole, i.e., they do not represent the ground-state spin state for these compounds (but conserves for early transition metal compounds). The dipole selection rules make the spectra strongly dependent on the symmetry of the initial state of the Co ions. According to [33–35], in a high-spin state the exchange coupling between the core-hole and 3*d* electrons tends to reduce noticeably the branching ratio from ½, while in the case when the Co ions mainly have the local low-spin state character the branching ratio differs on ½ only slightly. Analysis of the values obtained for studied BSCF with partial Nb substitution allows one to conclude that the ratio L_2/L_3 is 0.4 in all the samples except BSCFN10 indicating that the Co ions in these samples mainly have the local low-spin state character (Co^{3+} state). In the sample BSCFN10, Co ions mainly have the local high-spin state character (Co^{2+} state). The observed change in the branching ratio L_2/L_3 is an additional proof related to change in the oxidation state of the Co atom in the BSCFN10 sample.

It should be mentioned that Fe $L_{2,3}$-absorption spectra of the same BSCF structure were also studied. However, the joint analysis of Fe $L_{2,3}$-absorption spectra measured for BSCF structure with different Nb substitution did not reveal noticeable changes in the spectra that agree well with concepts of the role of the Fe atom in the BSCF structure: in the perovskite oxide BSCF the Fe atoms in contrast to the Co atoms are more resistant to changes in the oxidation state [9]. For this reason the Fe $L_{2,3}$-absorption spectra are not discussed in the current paper.

As was mentioned above, the lowering of the element oxidation state leads to increase of the ionic radius. The ionic radii of Co^{3+}- and Co^{2+}- oxidation states are 0.0545 nm (low spin) and 0.0745 nm (high spin) [36]. According to the Goldschmidt tolerance factor [3], the increase of the ionic radius B caused by lowering the oxidation state of B cation should stabilize the cubic phase of BSCF structures. Thus it is more reasonable to expect phase stabilization in the BSCF sample with 10% Nb substitution, for which the change in the oxidation state from Co^{2+}/Co^{3+} aside to Co^{2+} was established.

The exceptional behavior of BSCFN10 might be confirmed by the results from XRD measurements, see Fig. 3.

All reflections can be indexed by the cubic perovskite structure with a Pm-3m space group. The powder containing 10% Nb on the B-site, BSCFN10 reveals qualitatively different diffraction patterns than the other three powders BSCFN05, BSCFN15 and BSCFN20.

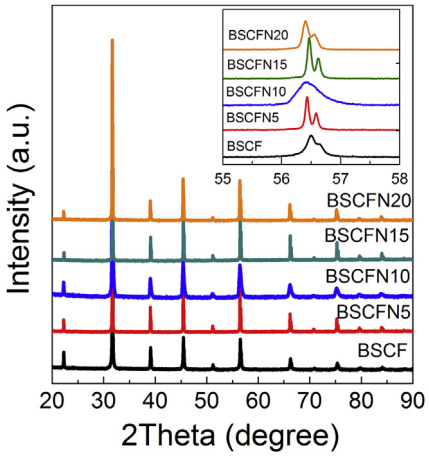

Fig. 3. XRD patterns of Nb substituted BSCF systems. The (211) reflection is shown in the inset.

While the reflections of the latter three powders reveal sharp reflections with peaks split into $K_{\alpha 1}$ and $K_{\alpha 2}$ sub-peaks, this kind of splitting is not observed for BSCFN10. Instead, BSCFN10 reveals broad reflections which point to either crystallite sizes on the nm scale, i.e., to crystallites with mean size below 100 nm, or to a distribution in chemical composition causing a variety of lattice parameters and thus broadening of lattice reflections. The origin of the peak broadening in BSCFN10 is not quite clear and the peak broadening observed for BSCFN10 is in disagreement to the results from XRD measurements of Fang et al. [12] which yielded an XRD pattern with small peak widths for all four powders, BSCFN05, BSCFN10, BSCFN15 and BSCFN20. Additional treatment of BSCFN10 at 1000 °C for 11 h caused slight narrowing of the diffraction peaks indicating increase in grain size, decrease of stresses or homogenization of chemical fluctuations. The structure remained, however, very different from those of the other powders.

Further evidence for the exceptional structure of BSCFN10 is given by neutron diffraction measurements which revealed an orthorhombic crystal structure with a Pnma space group in contradiction to the XRD results of Fang et al. [12]. Hence, further research is required to solve the puzzling structure of BSCFN10.

4. Conclusions

The mixed electronic ionic perovskite oxide BSCF with partial Nb substitution (5%–20%) for Fe and Co on the B-site has been studied by the NEXAFS technique. Joint analysis of the Co L_3-absorption spectra of Nb substituted BSCFN, CoO- and Co_3O_4- structures testified that only in the BSCFN10 samples does Co occur in the oxidation state close to Co^{2+}. In all other structures Co atoms are rather characterized by mixed oxidation states Co^{2+}/Co^{3+}.

Acknowledgment

The authors acknowledge financial support from the German-Russian Interdisciplinary Science Center (G-RISC, DAAD, projects P-2013a-8, P-2014a-11). We thank HZB for the allocation of synchrotron radiation beamtime. Support from Helmholtz-Association through the Helmholtz-Alliance MEM-BRAIN is also gratefully acknowledged.

References

[1] Z.P. Shao, S.M. Haile, Nature 431 (2004) 170–173.
[2] W. Zhou, R. Ran, Z. Shao, J. Power Sources 192 (2009) 231–246.
[3] V.M. Goldschmidt, Gesetze Kryst. Naturwissenschaften 14 (1926) 477–485.
[4] S. McIntosh, J.F. Vente, W.G. Haije, et al., Solid State Ion. 177 (2006) 1737–1742.
[5] Y. Li, H. Zhao, N. Xu, et al., J. Membr. Sci. 362 (2010) 460–470.
[6] B. Liu, Y. Zhang, L. Tang, Int. J. Hydrog. Energy 34 (2009) 435–439.
[7] S. Zeljković, T. Ivas, S. Vaucher, et al., J. Serb. Chem. Soc. 79 (9) (2014) 1141–1154.
[8] M.M. Kuklja, Y.A. Mastrikov, B. Jansang, E.A. Kotomin, J. Phys. Chem. C 116 (35) (2012) 18605–18611.
[9] M. Arnold, Q. Xu, F.D. Tichelaar, A. Feldhoff, Chem. Mater. 21 (4) (2009) 635–640.
[10] K. Efimov, Q. Xu, A. Feldhoff, Chem. Mater. 22 (21) (2010) 5866–5875.
[11] F. Wang, T. Nakamura, K. Yashiro, et al., Solid State Ion. 262 (2014) 719–723.
[12] S.M. Fang, C.-Y. Yoo, H.J.M. Bouwmeester, Solid State Ion. 195 (2011) 1–6.
[13] Y. Cheng, H. Zhao, D. Teng, et al., J. Membr. Sci. 322 (2008) 484–490.
[14] P. Müller, M. Meffert, H. Störmer, D. Gerthsen, Microsc. Microanal. 19 (2013) 1595–1605.
[15] J. Stöhr, NEXAFS Spectroscopy, Springer-Verlag, Berlin, 1992.
[16] S.I. Fedoseenko, I.E. Iossifov, S.A. Gorovikov, et al., Nucl. Instrum. Methods Phys. Res. Sect. A 470 (2001) 84–88.
[17] J.-I.I. Jung, D.D. Edwards, J. Solid State Chem. 184 (2011) 2238–2243.
[18] V.I. Grebennikov, V.R. Galakhov, L.D. Finkel'shtein, et al., Phys. Solid State 45 (6) (2003) 1048–1055.
[19] J. Taftø, O.K. Krivanek, Phys. Rev. Lett. 48 (1982) 560.
[20] M. Magnuson, S.M. Butorin, J.-H. Guo, J. Nordgren, Phys. Rev. B 65 (2002) 205106.

[21] M.M. Schooneveld, R. Kurian, A. Juhin, et al., J. Phys. Chem. C 116 (29) (2012) 15218–15230.
[22] A.F. Wells, Structural Inorganic Chemistry, Clarendon Press, London, 1950.
[23] F. Morales, F.M. De Groot, P. Glatzel, et al., J. Phys. Chem. B 108 (41) (2004) 16201–16207.
[24] U. Fano, J.W. Cooper, Rev. Mod. Phys. 40 (1968) 441.
[25] Y. Tanabe, S. Sugano, J. Phys. Soc. Jpn. 9 (1954) 753–766.
[26] A.B.P. Lever, Inorganic Electronic Spectroscopy, second ed., Elsevier, Amsterdam, The Netherlands, 1984.
[27] M.-Y. Li, P. Shen, Mater. Sci. Eng. B 111 (1) (2004) 82–89.
[28] D. Bazin, I. Kovács, L. Guczi, et al., J. Catal. 189 (2000) 456–462.
[29] S. Zhang, J.-j. Shan, Y. Zhu, et al., J. Am. Chem. Soc. 135 (2013) 8283–8293.
[30] B.T. Thole, G. Van der Laan, Phys. Rev. B 38 (3) (1988) 3158.
[31] R. Laskowski, P. Blaha, Phys. Rev. B 82 (2010) 205104.
[32] C. Suzuki, J. Kawai, H. Adachi, T. Mukoyama, J. Chem. Phys. 247 (3) (1999) 453–470.
[33] T. Mizokawa, L.H. Tjeng, P.G. Steeneken, et al., Phys. Rev. B 64 (2001) 115104.
[34] F.M. De Groot, J.C. Fuggle, B.T. Thole, G.A. Sawatzky, Phys. Rev. B 42 (1990) 5459–5468.
[35] J.L. Chen, Y.S. Liu, C.-J. Liu, et al., J. Alloys Compd. 529 (2012) 8–11.
[36] H.S.C. O'Neill, A. Navrotsky, Am. Miner. 68 (1983) 181–194.